Astron. Astrophys. 324, 763–769 (1997)

ASTRONOMY
AND
ASTROPHYSICS

Chromospheric polarity reversals on sunspots

Are they consistent with weak line emission?

J. Sánchez Almeida

Instituto de Astrofísica de Canarias, E-38200 La Laguna, Tenerife, Spain

Received 8 November 1996 / Accepted 10 February 1997

Abstract. Photospheric and chromospheric solar magnetograms sometimes show opposite polarity. This intriguing phenomenon is associated with the emergence of magnetic flux and with nearby, but not necessarily superposed, flaring activity. Despite the fact that there may be different explanations, it is shown here that the observed reversals are consistent with weak flare-like line emission all over the reversed polarity regions. Although this emission does not show up as a flare in filtergrams, it exhibits itself as a polarity reversal of the chromospheric magnetograms. If this interpretation were correct, the reversal would not correspond to a real flip of the magnetic field direction from the photosphere to the chromosphere. It would be an artifact due to radiative transfer effects. Observations to support or discard this hypothesis are briefly pointed out.

Key words: line: profiles – polarization – Sun: chromosphere – Sun: flares – Sun: magnetic fields – sunspots

1. Introduction

In a very careful paper, Wang & Shi (1992) describe the birth and subsequent evolution of a sunspot whose magnetic polarity reverses from the photosphere to the chromosphere. This intriguing phenomenon is by no means uncommon; the systematic investigation by Li et al. (1994) yields 680 of such reversals out of 300 pairs of magnetograms. According to the authors cited above, Chen, Ai, Zhang & Jiang (Chen et al. 1989) were the first to report the very same phenomenon, which will be denoted here by the CAZJ-reversal.

A proper knowledge of the chromospheric magnetic fields is basic for understanding the external layers of the Sun, in particular, the corona and its influence on the Earth environment. The chromosphere is the higher layer where routine magnetic field determinations are feasible. From there upwards one has to resort to extrapolations. The puzzling CAZJ-reversal offers a sound opportunity for testing and enlarging our knowledge of the chromosphere. Maybe, the CAZJ-reversal points out a novel and tangled magnetic field topology which puts face to face field lines of opposite polarities. On the contrary, it may not necessarily imply a real leap of the magnetic field vector from the photosphere to the chromosphere. An example of the first approach for deciphering the riddle is provided by Liu et al. (1995). Here I try the second way, i.e., probing whether the observations may be compatible with unipolar magnetic atmospheres having chromospheric-like temperature (or source function) rises. The CAZJ-reversal may be revealing either the complexity of chromospheric magnetic fields or difficulties in the interpretation of chromospheric magnetograms. In any case, pinning down its cause will provide valuable new information.

An emission feature in the core of the chromospheric line may give rise to chromospheric and photospheric magnetograms having opposite signs. This possibility was indeed explored and then discarded in the papers by Wang & Shi (1992), Dara et al. (1993) and Li et al. (1994). The argument was always that, usually, regions of reversed polarity coincide with dark features of the chromospheric filtergrams. Therefore, *the polarity reversal is not caused by the reversal of the line profile from absorption to emission* (Wang & Shi 1992). Here I revise this argumentation pointing out that variations within a filtergram just show differences among the flux of photons emitted by different regions. Line shapes in dark features like sunspots can suffer drastic changes and still, because of the low sunspot emission, not be revealed in filtergrams. On the contrary, magnetograms exhibit relative quantities (basically the degree of circular polarization). Consequently, local changes of the spectral lines promptly modify the magnetogram signals. The Sun can actually generate chromospheric lines having a weak emission core which a) produces photospheric and chromospheric magnetograms of opposite signs, and b) does not show up in filtergrams.

The present work elaborates the argument sketched above. I put forward a simple model sunspot which reproduces the main properties of the CAZJ-reversal. Sect. 1.1 summarizes the observations to be explained. Sect. 2.1 describes the spectral synthesis employed in synthesizing magnetograms and filtergrams.

Send offprint requests to: J. Sánchez Almeida

The model sunspot and the resulting magnetograms and filtergrams are discussed in Sect. 2.2. Observations and simulation are compared in Sect. 3. Finally, Sect. 4 considers an obvious observational test to validate or invalidate the interpretation of the CAZJ-reversal proposed here.

1.1. Summary of observations concerning the CAZJ-reversal

The simulation described in the paper are aimed at reproducing the CAZJ-reversal. For the sake of clarity, this section specifies those observations to be understood. This summary has been distilled from the following references: ⋆ Wang & Shi (1992), ○ Dara et al. (1993), ● Li et al. (1994), ◇ Liu et al. (1995), ⊗ Zhang (1996) (symbols in the list identify the appropriate references).

1. The circular polarization has opposite signs depending on whether it is measured in the flank of a photospheric line or a chromospheric line. Most observations refer to the pair Fe I 5324 Å (photosphere) and H_β (chromosphere) ⋆●◇ ⊗, although this is not always the case ○.
2. No obvious brightening of the chromospheric filtergrams sets in together with the onset of the reversal ⋆ ● ◇ ○ ⊗. However, there is continuous flare activity (i.e., brightenings in the filtergrams) around regions where the reversed polarity occurs. Sometimes the location of the reversal itself corresponds to a flare kernel ⋆ ● ◇.
3. The reversals seem to occur on dark structures, either on sunspot umbrae or penumbrae ⋆ ● ○ ⊗.
4. Regions which show reversals are characterized by a very fast increase of both the line-of-sight magnetic flux ⋆ ● ◇○, and the transverse component of the vector magnetic field ⋆ ● ◇.
5. The reversals are normally associated with H_β redshifts. The peak velocity does not coincide with the reversed polarity structures, though ⋆●. The region studied by Liu et al. (1995) shows blue-shifts.
6. The CAZJ-reversal is not necessarily a transient phenomenon. It may last for hours or days ⋆ ● ◇. Sometimes, it disappears to show up again ⋆●.

2. The model polarity reversal

2.1. Description of the spectral synthesis

A comprehensive simulation of the CAZJ-reversal requires solving the NLTE radiative transfer problem in a flaring magnetized chromosphere. This extraordinarily complex issue goes beyond the scope of this work but, fortunately, the basic ingredient is simple. One just needs lines having emission cores of various degrees. The modeling put forward here employs a very simple treatment of the radiative transfer which, however, handles emission lines, i.e., the NLTE solutions of the radiative transfer equation for polarized light by Lites et al. (1988). Using the notation of Murphy (1990), these solutions can be written down as

$$\begin{aligned}\mathbf{I} = \; & B_0\mathbf{u} + \mu B_1(\mathbb{1}+\eta_0\Phi)^{-1}\mathbf{u} + \\ & A\mathbf{u} - A(\mathbb{1}+\tfrac{\eta_0}{1+\mu\epsilon}\Phi)^{-1}\mathbf{u},\end{aligned} \tag{1}$$

where the symbols, μ, η_0, $\mathbf{I}$ and $\mathbf{u}$ represent, respectively, the cosine of the heliocentric angle, the ratio line-to-continuum absorption coefficient, the Stokes vector $(I,Q,U,V)^\dagger$, and $(1,0,0,0)^\dagger$. (Superscripts † denote transpose matrices.) The polarization described by (1) obeys the radiative transfer equation

$$\mu\frac{d}{d\tau}\mathbf{I} = (\mathbb{1}+\eta_0\Phi)\mathbf{I} - (S_c + S_l\eta_0\Phi)\mathbf{u}, \tag{2}$$

under various simplifying assumptions. $\mathbb{1}+\eta_0\Phi$ is the so-called absorption matrix which, as in a standard Milne-Eddington atmosphere, is assumed to be constant. In addition, the continuum source function S_c, and the line source function S_l, vary with continuum optical depth τ as

$$\begin{aligned}S_c = \; & B_0 + B_1\tau, \\ S_l = \; & B_0 + B_1\tau + A\exp(-\epsilon\tau).\end{aligned} \tag{3}$$

S_l allows for a chromospheric rise (an increase towards small optical depths) whose amplitude is controlled by the parameter A (>0). On the other hand, ϵ ($\gg 1$) sets the optical depth where this rise starts. Examples of S_l are given in Fig. 5. In addition to the explicit parameters in Eqs. (2) and (3), the spectrum (1) also depends on the Doppler width of the line v_D, the damping parameter a, the magnetic field strength B, azimuth ϕ, and inclination γ, and, finally, the effective Landé factor g_{eff}. This implicit dependence is concealed within Φ (see., e.g., Landi Degl'Innocenti 1992).

Stokes profiles[1] provided by Eq. (1) are employed through all the simulation. However, there is an LTE solution of Eq. (2) which, in practice, gives the same polarization. In the case that

$$S_c = S_l = B_0 + B_1\tau + A\exp(-\epsilon\tau), \tag{4}$$

the solution of Eq. (2) becomes (Landi Degl'Innocenti 1992)

$$\begin{aligned}\mathbf{I} = \; & B_0\mathbf{u} + \mu B_1(\mathbb{1}+\eta_0\Phi)^{-1}\mathbf{u} + \\ & A\mathbf{u} - Af(\mathbb{1}+\tfrac{\eta_0}{1+\mu\epsilon}\Phi)^{-1}\mathbf{u}, \\ f = \; & 1 - 1/(1+\mu\epsilon).\end{aligned} \tag{5}$$

This Stokes vector and (1) are virtually the same for the type of atmosphere employed here, i.e., with $\epsilon \gg 1$ and so having $f \simeq 1$. Consequently, the treatment of the radiative transfer along the paper corresponds to either of two possibilities, a) NLTE solutions for lines whose source functions increase with height (3), or b) LTE solutions having increasing temperature with height compatible with (4).

Once synthetic Stokes I and V profiles are available, filtergrams F and magnetograms M can be straightforwardly computed. If the narrow-band filter which characterizes the measurement has a transmission T, the signals are given by,

$$\begin{aligned}F = \; & \int IT d\lambda, \\ M = \; & (\int VT d\lambda)/F, \\ B_{LOS} = \; & CM.\end{aligned} \tag{6}$$

[1] Employing the usual nomenclature, the term Stokes profiles stands for the variation with wavelength of the four Stokes parameters.

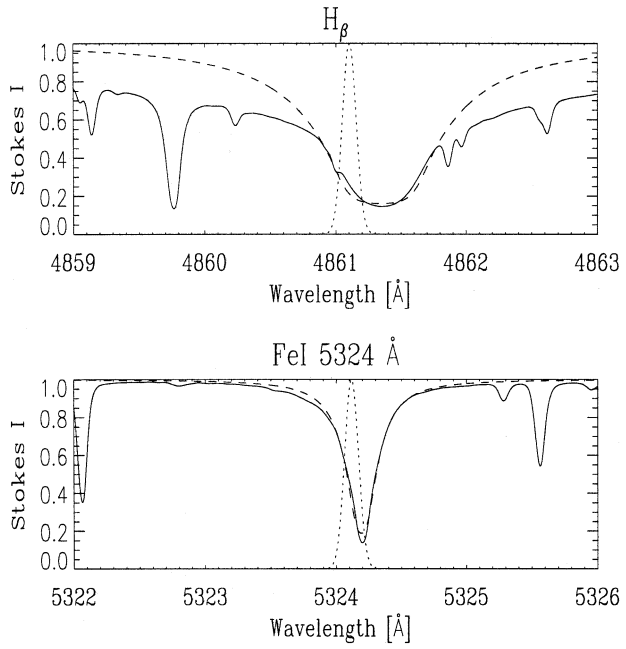

Fig. 1. Observed Stokes I profiles of H_β and Fe I 5324 Å (the solid lines, from Delbouille et al. 1973). By fitting these quiet Sun observations with synthetic profiles (the dashed lines), we set atomic parameters for the simulation (see text for details). The dotted lines represent the transmission of narrow-band filters used in simulating filtergrams and magnetograms.

Table 1. Set of parameters employed in the simulation. λ_0, λ_f and I_c represent, respectively, the central wavelength of the lines, the peak wavelengths of the narrow-band filters, and the continuum intensities referred to the quiet Sun. See the text for other symbols.

	H_β	Fe I 5324 Å
atomic parameters		
η_0	100.	50.
λ_0 [Å]	4861.34	5324.19
a	0.2	1.0
v_D [mÅ]	150.	25.
g_{eff}	1.0[4]	1.5
.....	.....	.....
narrow-band filters		
$\lambda_f - \lambda_0$ [mÅ]	-240.	-75.
FWHM [mÅ]	125.	125.
.....	.....	.....
model atmospheres		
$B_1/(B_0 + B_1)$	0.85	0.85
ϵ	100.	100.
A	0.12[1],0.35[2]	0.12[1],0.35[2]
μ	0.7	0.7
γ[3]	46°	46°
Maximum B [G]	2000.	2000.
Umbral radius	8.″	8.″
Penumbral radius	20.″	20.″
Umbral I_c	0.2	0.2
Penumbral I_c	0.7	0.7

[1] umbra
[2] penumbra
[3] taken so that $\cos\gamma = \mu$
[4] actually ~ 1, Casini & Landi Degl'Inoccenti (1994)

The symbol λ stands for the wavelength and the integrals span whole spectral lines. Sect. 2.2 describes a procedure to compute the calibration constant C, i.e., to transform degrees of circular polarization M into longitudinal magnetic field strengths B_{LOS}.

2.2. Synthetic filtergrams and magnetograms

In order to produce filtergrams and magnetograms out of Eqs. (1) and (6), one has to provide figures for a) the atomic parameters of the spectral lines, b) the model atmospheres, and c) the narrow-band filters. This section is aimed at critically describing the origin of the data set employed here. In addition, the final paragraphs refer to the synthetic magnetograms and filtergrams, and how they are weakly dependent on the actual data.

Table 1 collects the whole set of parameters. Note that none of them but A and ϵ are free parameters. They have not been tuned to match observations but, instead, they were chosen to represent the type of measurements showing the CAZJ-reversal.

The lines H_β and Fe I 5324 Å were selected as this pair is most often used in observing the reversal. The atomic parameters of these lines have been set by fitting Stokes I profiles observed in the quiet Sun (Fig. 1). In the case of zero magnetic field and no chromosphere, the Stokes I profiles (1) just depend on B_0, B_1, η_0, a and v_D, which are the parameters deduced from the fitting. The Doppler widths in Table 1 are set by the thermal Doppler widths of the two species (H and Fe) at 6000 K, i.e., a representative photospheric temperature (e.g., Allen 1976). B_1 and B_0 are unambiguously deduced from continuum intensity and line-core intensity. There is some cross-talk between a and η_0, which is solved by choosing η_0-of-H_β and η_0-of-Fe I 5324 Å as different as possible. This separates the formation heights of the two lines so as to enlarge the distinction between the chromospheric line and the photospheric line. Note that the Stark-broadened wings of H_β are not reproduced. However, the wings do not affect magnetograms or filtergrams, which come from wavelengths close to the line core (see the filters in Fig. 1).

For simplicity, the transmission curves of the narrow-band color filters have been assumed to be Gaussian (i.e., T in Eq. [6] is a Gaussian). The central wavelength and the full-width-half-maximum (FWHM) of the transmission about H_β have been taken from Liu et al. (1995). The central wavelength for Fe I 5324 Å is also mentioned in Liu et al. (1995). Lacking the actual FWHM value for this line, I adopted that used for H_β.

Observations show that the CAZJ-reversal occurs on sunspots (see item # 3, Sect. 1.1). A model sunspot has been laid out to conform to an average observed sunspot (compare Table 1 with, e.g., Allen 1976). The continuum intensity of this model sunspot is presented in Fig. 2. The original step-like ra-

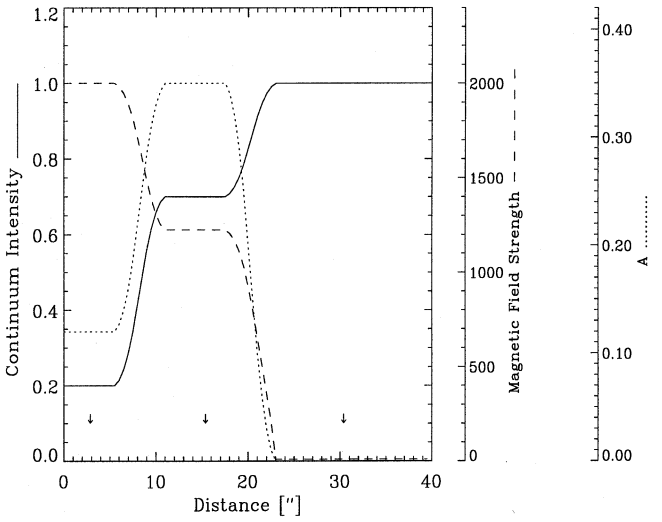

Fig. 2. Variation across the model sunspot of continuum intensity (the solid line), magnetic field strength (the dashed line) and chromospheric rise factor A (the dotted line). The umbral and penumbral radii have been set to $8''$and $20''$, respectively. The distance from the sunspot axis is measured in arcsec.

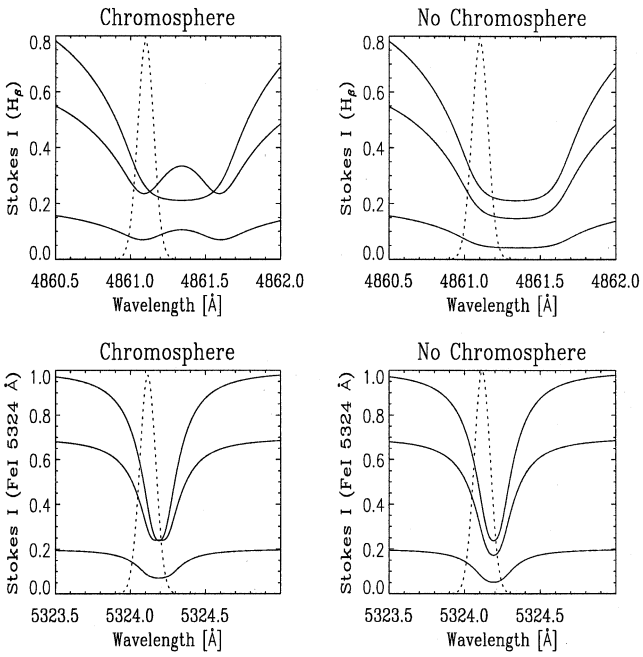

Fig. 3. Stokes I profiles corresponding to the umbra (lowest intensities), the penumbra, and the quiet photosphere of the model sunspot (see arrows in Fig. 2). The dotted lines represent the transmission of the narrow-band filters used to simulate filtergrams and magnetograms. Note the emission core of H_β in the umbral and penumbral profiles (chromosphere). The Stokes I profiles are normalized to the quiet Sun continuum intensity.

dial variation reflected in Table 1 has been smoothed here with a $4''$ running spatial filter. (This filtering obeys purely aesthetic reasons.) The simulation supposes B_1/B_0 to be that obtained from the quiet Sun fitting (Table 1). As far as the radial variation of the magnetic field strength B is concerned, I set it from the empirical linear relationship between B^2 and the continuum intensity (Martínez Pillet & Vázquez 1993). A maximum magnetic field strength and the previous relationship provide the whole radial variation of the magnetic field strength (Fig. 2). The magnetic field direction of the whole sunspot is assumed to be vertical. Assuming vertical penumbral magnetic fields is very unrealistic. However, this assumption facilitates modeling the sunspot off the disk center (γ becomes the heliocentric angle) and, what is really important, the actual magnetic field inclination does not modify the existence of a polarity reversal. We come back to this point later.

Let me now describe the tuning of the only two free parameters, ϵ and A. These control the exponential rise of the source function (3). ϵ has been set so that the contribution of the exponential function starts where the line center opacity of H_β, τ_l, equals one ($\tau\epsilon \leq 1$ for the exponential to contribute; I set $\epsilon \sim \eta_0$, which leads to $\tau_l \sim \eta_0\tau \sim 1$ when $\tau\epsilon \sim 1$). The amplitude of the chromospheric rise A has been adjusted so that a) the H_β filtergram does not show up bright in the penumbra and b) the umbral reversal is a few hundred Gauss. None of these requirements is very severe and one can produce images showing the CAZJ-reversal for many other combinations of values.

Once the radial variation of the relevant parameters is set, Eq. (1) yields the line polarization corresponding to each radial position across the sunspot. Three representative Stokes I and Stokes V profiles are plotted in Figs. 3 and 4. Both spectra with and without chromosphere are shown for comparison (no chromosphere means setting $A = 0$ in the model atmospheres described above). The arrows in Fig. 2 point out which sunspot radii the profiles belong to. Source functions corresponding to these profiles are given in Fig. 5. The variation of the magnetograms and filtergrams along the sunspot radius was deduced by application of Eq. (6) to the synthetic profiles. The images in Figs. 6 and 7 were subsequently constructed assuming rotational symmetry about the sunspot's axis and applying the appropriate foreshortening. (I have chosen $\mu = 0.7$ as this value roughly corresponds to the location of the reversal described by Wang & Shi 1992). Each image has been scaled so that it fits the gray levels of the printer (some 100). In the case of the filtergrams (both H_β and continuum), the scale goes from zero, for zero intensity, to the maximum intensity. On the other hand, the magnetograms span from $\pm$ the maximum absolute value of the magnetogram signal. The grey tone surrounding the sunspot corresponds to no magnetic field, consequently, points darker and lighter than this background show opposite polarities. As we will discuss in Sect. 3, Fig. 6 shows the CAZJ-reversal while Fig. 7 does not. The latter has been produced with the same model atmospheres but removing the chromospheric rise ($A = 0$). Upon removal of the chromosphere, the only significant modification is the disappearance of the chromospheric polarity reversal.

The degree of circular polarization and the magnetogram magnetic field are, except for a calibration constant, the very same quantity (Eq. [6]). Observers have quantified the strength

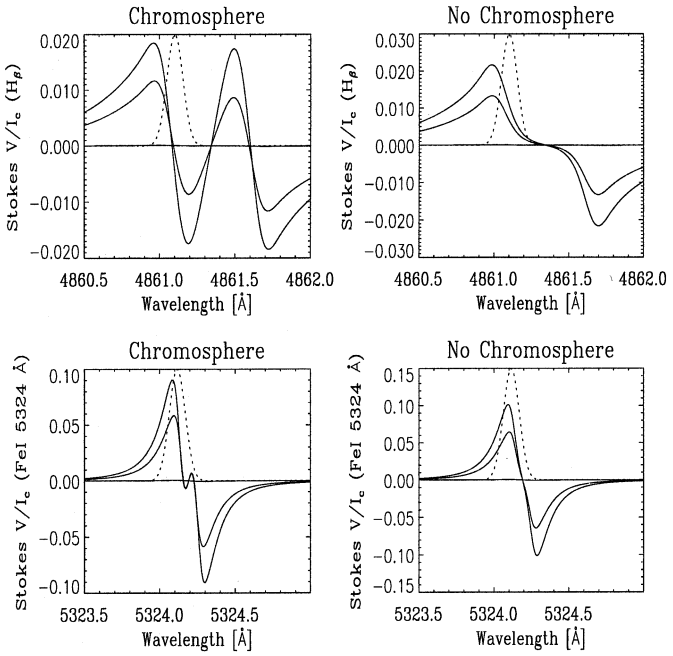

Fig. 4. Stokes V profiles of the model sunspot normalized to the local continuum (I_c). The Stokes V under the dotted lines roughly provides the magnetogram signals. Note that a) the average polarizations of H_β and Fe I 5324 Å have opposite signs (chromosphere), b) due to the continuum normalization the largest Stokes V/I_c correspond to the umbral profiles, and c) the quiet Sun profiles yield no polarization.

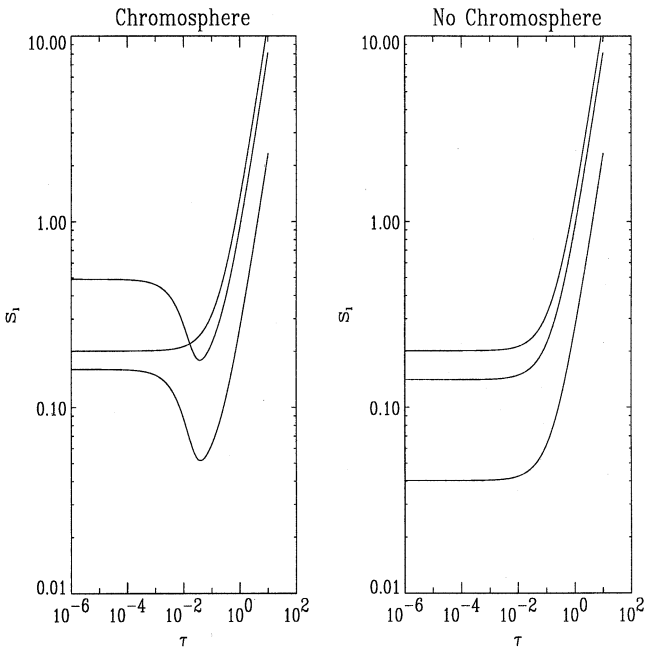

Fig. 5. Line source function corresponding to the synthetic spectra in Figs. 3 and 4. τ stands for the continuum optical depth. S_l at $\tau \sim 1$ reveals whether the various source functions correspond to the umbra (smaller), the penumbra, or the quiet Sun (larger).

of the CAZJ-reversal in G, so the present simulation was transformed to G for comparison. I used the relationship between the magnetogram signal M and the true longitudinal magnetic field strength $B\cos\gamma$ when $A = 0$ (Stokes profiles and corresponding source functions are shown in Figs. 3, 4 and 5, right-hand columns). The relationship between the two quantities is fairly linear (Fig. 8, top), the slope being the calibration constant. Calibration constants thus obtained were subsequently used to calibrate the magnetograms. The bottom plot in Fig. 8 shows the apparent longitudinal magnetic field of the model sunspot. The maximum reversed polarity reaches -300 G, in good agreement with the figures quoted by Wang & Shi (1992) or Liu et al. (1995).

The polarity reversal modeled here is barely dependent on the parameters which describe the lines and atmospheres. Filtergrams and magnetograms resembling Fig. 6 result from very different combinations of model parameters. The only essential ingredients are a) η_0-of-H_β > η_0-of-Fe I 5324 Å, b) $A > 0$, and c) $\epsilon \sim 1/\eta_0$-of-H_β. As already stated at the beginning of this section, the parameters in Table 1 were chosen to represent realistic solar values. γ in penumbrae represents the exception, however, its actual value does not modify the polarity reversal. To the first order, $\cos\gamma$ just scales the degree of circular polarization produced by a line. Therefore, if H_β and Fe I 5324 Å yield opposite polarities in a given atmosphere, they do so independently of the magnetic field inclination.

3. Comparison of the model reversal with observations

The magnetograms of H_β and Fe I 5324 Å in Fig. 6 show opposite polarity. The corresponding H_β filtergram does not show a brightening associated with the reversed polarity region (both umbra and penumbra are darker than the surrounding quiet Sun). Even more, the magnetic field strength of the reversal (or, equivalently, the degree of circular polarization) is similar to those reported in the literature (Fig. 8, bottom). Consequently, the present simulation mimics the two main observations associated with the CAZJ-reversal (items #1 and #2 in Sect. 1.1). What about other properties of the reversal which are not direct outcomes of the simulation? Let me speculate that the CAZJ-reversal, as well as these other properties, may be side effects of the magnetic flux emergence (Sect. 1.1, item # 4). It is well documented that the flux emergence is associated with redshifts in the chromosphere and photosphere (e.g., Zwaan 1985). This would account for property #5 (in fact, Wang & Shi 1992 already pointed out that the observed velocity pattern is consistent with that of an emerging flux region). Similarly, an increase of the transverse magnetic field accompanies any magnetic flux emergence of inclined field lines. Again, this would qualitatively explain property #4.

The present simulation assumes H_β to show a weak emission at the reversed polarity regions. Does this assumption sound reasonable? Regions about the reversals present frequent flares (item #2, Sect. 1.1). Flares are known to produce line emission all over the solar spectrum (see, e.g., Švestka 1972). It sounds natural that similar-but-weak line emission actually takes place

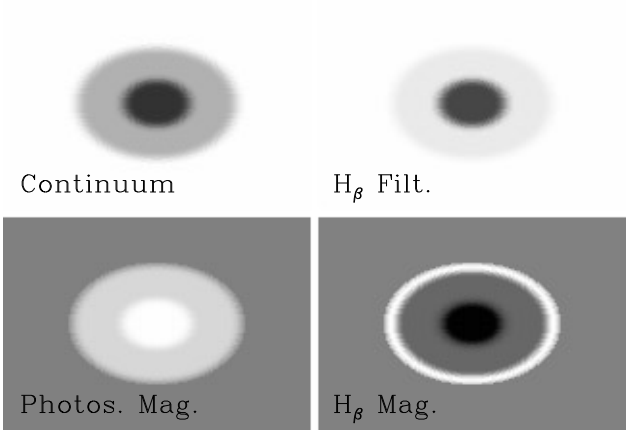

Fig. 6. Filtergrams and magnetograms showing the CAZJ-reversal, i.e., chromospheric (H_β) and photospheric (Fe I 5324 Å) magnetograms having opposite polarity while the chromospheric filtergram does not flare. The background about the sunspot has no magnetic field, therefore, regions of the magnetograms lighter and darker than this background represent opposite polarities.

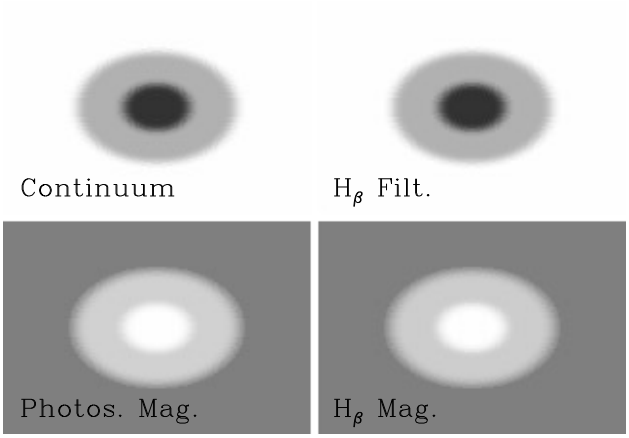

Fig. 7. Same as Fig. 6 but without chromospheric rise. The basic difference is the disappearance of the polarity reversal of the H_β magnetogram.

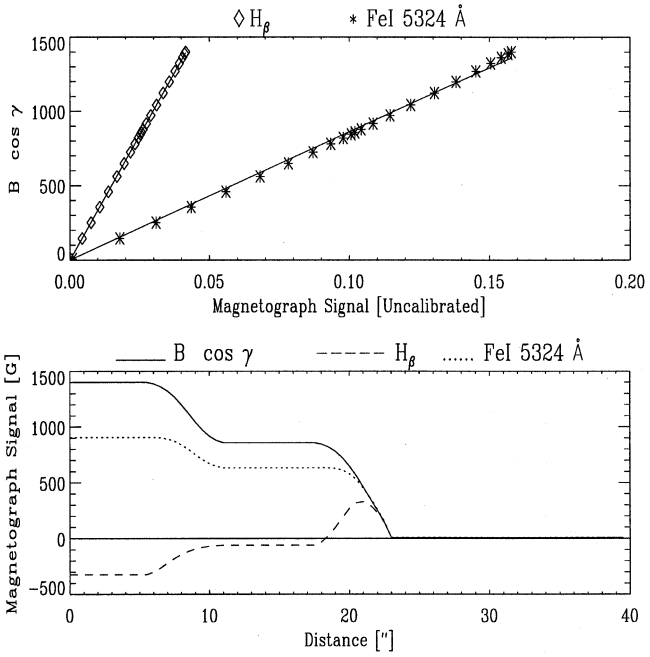

Fig. 8. Upper panel: real longitudinal magnetic field versus magnetogram signal assuming no chromosphere. The straight lines represent linear fits whose slopes provide the calibration constants for the magnetograms. Lower panel: actual magnetogram signal (once calibrated) versus position along the sunspot radius. Note the reversed polarity of H_β in the umbra and most of the penumbra.

in reversed polarity regions. The persistence and recurrence of many CAZJ-reversals (item #6, Sect. 1.1) may be associated with their appearance on sunspots. Umbral flares are known to be long lasting and recurrent (see Tang 1978). Maybe the reversals belong to the same family of flare activity, except for being much more frequent and less energetic.

According to Li et al. (1994), an important fraction of the observed reversals corresponds to reversals of the photospheric magnetograms. Contrary to what it is modeled here, Fe I 5324 Å is now the line showing the wrong polarity (i.e., Fe I 5324 Å in the reversed polarity region has a sign opposite to that in the nearby surroundings). Such a situation is still compatible with our modeling if H_β and Fe I 5324 Å interchange their roles. This may happen if the line opacity of Fe I 5324 Å becomes larger than the opacity of H_β. Such a possibility is indeed plausible considering that a) the opacities of H_β and Fe I 5324 Å in the quiet Sun are not very different (see Table 1), and b) we may be dealing with complex flaring atmospheres having very abnormal stratifications. The required change of roles may also be achieved if the line source functions of the two lines differ, specifically, if the source function of H_β does not show a chromospheric rise while that for Fe I 5324 Å does. The two source functions are taken to be the same in Sect. 2.2.

4. Wind-up and test

This paper shows how the CAZJ-reversal (photospheric and chromospheric magnetograms having opposite polarities, while filtergrams do not flare) is consistent with weak flare-like emission of the chromospheric line. At present, this possibility cannot be ruled out from observational grounds.

Stokes I and V spectro-polarimetry of H_β and Fe I 5324 Å on reversed polarity regions should provide a final answer. If emission at Stokes I line core shows up then the thesis discussed here is correct. Otherwise, the CAZJ-reversal requires an explanation based on actual reversal of the magnetic field direction along the line-of-sight. If our hypothesis proves to be correct, detecting reversed polarities in magnetograms may be a way of monitoring weak flare activity, invisible in standard chromospheric filtergrams. If it were correct, the existence of the CAZJ-reversal can also be used to favor spectro-polarimetry for chromospheric magnetic field determinations. Spectro-polarimetry

allows emission cores to be detected and taken into account in magnetic field estimates.

Acknowledgements. Thanks are due to Javier Trujillo Bueno for a critical reading of the original manuscript. The suggestions by Franz Kneer greatly improved the presentation of the paper. This work has been partly funded by the Spanish DGYCIT under project 95-0028-C.

References

Allen C. W., 1976, Astrophysical Quantities, The Athlone Press, London
Casini R., Landi Degl'Innocenti E., 1994, A&A 291, 668
Chen J., Ai G., Zhang H., Jiang S., 1989, Publ. Yunnan Obs., Special Issue 1, 108
Dara H. C., Koutchmy S., Alissandrakis C. E., 1993, A&A 277, 648
Delbouille L., Roland G., Neven L., 1973, Photometric atlas of the solar spectrum, Institut d'Astrophysique de L'Université de Liège
Landi Degl'Innocenti E., 1992, in: Solar observations techniques and interpretation, eds. F. Sánchez, M. Collados & M. Vázquez, Cambridge University Press, Cambridge, 71
Li W., Ai G., Zhang H., 1994, Solar Phys. 151, 1
Lites B. W., Skumanich A., Rees D. E., Murphy, G. A., 1988, ApJ 330, 493
Liu Y., Srivastava N., Prasad D., Li W., Ai G., 1995, Solar Phys. 158, 249
Martínez Pillet V., Vázquez M.,1993, A&A 270, 494
Murphy G. A., 1990, NCAR Cooperative Thesis # 124, NCAR, Boulder
Ŝvestka Z., 1972, ARA&A 10, 1
Tang F., 1978, Solar Phys. 60, 119
Wang J., Shi Z., 1992, Solar Phys. 140, 67
Zhang H., 1996, ApJ 471, 1049
Zwaan C., 1985, Solar Phys. 100, 397

This article was processed by the author using Springer-Verlag LaTeX A&A style file *L-AA* version 3.